

# An investigation on layered birnessite type manganese oxides for battery applications

R. Renuka <sup>\*</sup>, S. Ramamurthy

Central Electrochemical Research Institute, Madras Unit, CSIR Madras Complex, Chennai 600 113, Madras, India

Received 12 June 1998; accepted 7 October 1999

## Abstract

Layered birnessite-type manganese oxide was prepared by a simple redox sol–gel reaction involving hydroxylamine and permanganate in alkaline medium. IR, XRD, Auger electron spectroscopy, EPR, TGA and cyclic voltammetric characteristics of the birnessites are presented. The birnessite was examined for its cathode performance in zinc-, magnesium- and lithium-based cells. Bismuth and lead exchanged birnessite show superior battery performance when compared with sodium and potassium precursors. The magnetoresistance pattern of the discharged birnessite (in Mg/Mg(ClO<sub>4</sub>)<sub>2</sub>) indicates a colossal magnetoresistance. This observation provides a scope for further studies of examining the applicability of magnetoresistance measurement in assessing the charge/discharge status of manganese oxides. Heat treatment of birnessite brings about distinct changes in the EPR and IR pattern. A correlation between the spectral features and electrochemical activity can be understood. © 2000 Elsevier Science S.A. All rights reserved.

**Keywords:** Birnessite; Sol–gel synthesis; Hydroxylamine–permanganate redox reaction; Battery performance; EPR; Magnetoresistance

## 1. Introduction

Birnessite, a  $\delta$ -MnO<sub>2</sub> is a poorly crystallized form of manganese dioxide characterized by a two-dimensional layered structure that consists of edge shared MnO<sub>6</sub> octahedra with cations and water molecules occupying the interlayer region. Birnessite is represented by a general formula, A<sub>x</sub>Mn<sub>2+y</sub>(H<sub>2</sub>O)<sub>z</sub> in which A represents an alkali metal cation [1–3]. The microporous nature of birnessite and its relative abundance in marine manganese nodules make it an active form of MnO<sub>2</sub> for use as a battery material [4–10]. The investigations of Yao et al. [11], Wroblowa [12] and Dzicciuch et al. [13] have demonstrated the usefulness of lead and bismuth birnessites for battery applications.

Sol–gel synthesis offers several advantages over conventional synthetic techniques [14] and is much sought after in the preparative chemistry of speciality materials. A problem faced in the sol–gel route to manganese oxides is the non-availability of suitable Mn(IV) molecular precursors in aqueous solutions. However, certain redox systems such as fumaric acid–KMnO<sub>4</sub> have effected the sol–gel synthesis of birnessites [15]. Similarly, birnessites have

been prepared by sol–gel redox reactions between permanganate and glucose [16,17]. In the present paper, we report the synthesis of the layered birnessite-type manganese oxides by a simple sol–gel redox reaction between permanganate and hydroxylamine in alkaline medium. The birnessite thus prepared is examined for its performance as a cathode material in zinc-, magnesium- and lithium-based battery systems.

## 2. Experimental

Unless otherwise specified, all chemicals used were E Merck GR grade products. Double distilled water was used in preparing the solutions.

### 2.1. Preparations of birnessite

A solution of 6 g of potassium permanganate in 50 ml of 5% KOH was added quickly to a solution of 10–12 g of hydroxylamine in 50 ml of 20% KOH; the resulting solution was vigorously stirred for about 3 min and then allowed to stand when a reddish brown sol formed which when left to remain at room temperature thickened to form a deep brown gel within about 2 h. Upon drying at 393 K, the gel yielded a porous black mass. Calcination of this

<sup>\*</sup> Corresponding author. Fax: +91-44-2352-456.

mass at 673 K gave a black powder. The powder was washed several times with distilled water and then dried at 393 K. The resulting black powder (yield = 2.3 g) was characterized to be a potassium birnessite.

Sodium birnessite was prepared in a similar manner using sodium permanganate in the place of potassium permanganate.

Ion-exchanged birnessites were prepared by shaking the sodium birnessite in the salt solution containing bismuth, lead or zinc ions. The choice of the sodium precursor was owing to the reported difficulty of exchanging potassium ions.

The analysis revealed a formula of  $K_{1.44}Mn_6O_{11.7} \cdot 1.5 H_2O$  for potassium birnessite;  $Na_4Mn_{14}O_{27} \cdot 9H_2O$  for sodium birnessite. A manganese oxidation state of, respectively, 3.72 and 3.57 was revealed by iodometric titration [18].

## 2.2. Analysis of potassium birnessite

IR spectra were recorded on a Shimadzu IR 408 spectrophotometer using KBr pellets (Fig. 1). Water content was ascertained from thermogravimetric measurement made on a Perkin Elmer Delta series TGA 7 instrument. Auger electron spectra were obtained using a Perkin-Elmer scanning microprobe. Elemental analysis was carried out using a GBC Avanta DB AAS instrument. X-ray diffraction pattern was obtained using a Philips X-ray diffractometer (Model 1140) using  $CuK\alpha$  radiation.

## 2.3. Battery performance evaluation

### 2.3.1. Magnesium and zinc cells

Aluminium–zinc–magnesium alloy, AZ31 sheet 0.015-m thick and zinc sheet, (99.9% purity), 0.03-m thick were, respectively, used for the magnesium and zinc anode. The cathode was made by mixing the birnessite (2.3 g, 0.7 A h) with colloidal graphite (15 wt.%) and 0.2 ml teflon binder

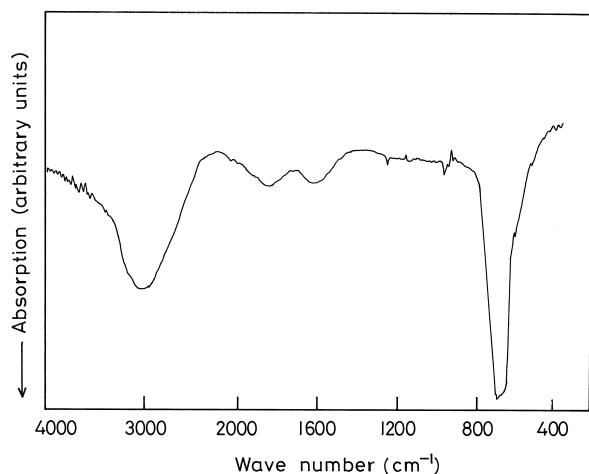


Fig. 1. IR spectrum of potassium birnessite.

which was then mounted on a nickel plated mild steel mesh ( $0.025 \times 0.040 \times 0.002$  m) and compacted using a hydraulic press. In a cell, a cathode plate was placed between two anode sheets and a pair of thin PVC wires pasted onto the inner side of the anode plates prevented direct contact of the cathode with the anode. A layer of cellophane was also interposed between the anode and the cathode. The electrolytes for the zinc cell was  $ZnCl_2/NH_4Cl$  (26 wt.%  $NH_4Cl$  + 8.8 wt.%  $ZnCl_2$  + 65.20% water + 0.2 wt.%  $Hg_2Cl_2$ ); the electrolyte for the magnesium cell was magnesium perchlorate (12.6 wt.%  $Mg(ClO_4)_2$  + 87.0 wt.% water + 0.4 wt.% barium chromate). The cell was connected in series to a variable resistor and in parallel to a voltmeter and the discharge was carried out at a constant current drain of 100 mA.

### 2.3.2. Zinc alkaline cells

For the zinc alkaline cell, the  $MnO_2$  (1.08 g, 0.3 A h) + 15 wt.% colloidal graphite + 0.2 ml teflon binder cathode blend was moulded under high pressure into a steel can which served as the cell container as well as positive terminal; a cellophane separator was kept inside the moulded cathode; a gel negative was prepared using 150 mesh zinc powder, 60.5 wt.%, 3 wt.%  $ZnO$ , 30 wt.%  $KOH$ , 3.5 wt.% mercuric chloride, 3 wt.% carboxyl methyl cellulose and a brass current collector. The discharge was carried out at a constant current drain of 100 mA. Reversible zinc alkaline cells have been constructed and tested using the Yao et al. procedure [11].

### 2.3.3. Lithium cells

Lithium perchlorate (Purum Fluka) was vacuum-dried at 433 K for 24 h. Propylene carbonate (Purum Fluka) stored over 4 Å molecular sieves (Linde, Union Carbide) for several days was dried over calcium oxide for 24 h and distilled under reduced pressure (1 mm of mercury). 1,3-dioxalane (Purum Fluka) was refluxed for 24 h with lead(IV) oxide, cooled and filtered. Xylene and more lead(IV) oxide were added and the mixture was fractionally distilled. The main fraction collected at 343 K was treated with xylene and sodium wire and then distilled. More sodium was added to the product and, finally, the sample boiling at 347 to 348 K was collected [19]. 1 M solutions of  $LiClO_4$  in 1:1 (v/v) mixture of propylene carbonate and dioxalane was used as the electrolyte; the water content in the electrolyte solution was 45 ppm as measured using a Photovolt Aquatest. The conductivity of 1 M  $LiClO_4$  solution in the 1:1 propylene carbonate and dioxalane mixture was  $8.7 \times 10^{-3} S cm^{-1}$ .

The cathode mix was prepared by intimately mixing, 0.135 g (0.04 Ah) birnessite (which was heat treated at 623 K) with 10 wt.% of colloidal graphite and 10 wt.% of teflon in the form of a colloidal suspension and drying the mixture at 373 K. Cathode pellets of dimension 0.02-m diameter and 0.002-m thickness were made by pressing the mix in a die under  $200 kg cm^{-2}$  pressure. This pellet was

then placed on an expanded mesh spot welded to the cathode cup. Pure lithium metal ingots (Cyprus Foote Mineral, USA) was shaped into circular discs of 0.0015-m thickness and 0.02-m diameter and swaged onto an expanded nickel mesh welded to the anode can. Celguard 2400 was used as the separator. The cell assembly was made inside a M Brawn (Germany) glove box flooded with argon and a 2450-type coin cell hardware in a 316-L stainless steel was used. Crimp sealing of the cells was done using a die mounted on a fly-press. The cell was discharged in a home-assembled discharge tester at 303 K and at a constant current drain of 10 mA.

#### 2.3.4. Impedance measurement

The fabricated Li cells were stored for 10 days before subjecting to the impedance measurement. A home-assembled spring-loaded impedance cell with two stainless steel disc electrodes with dimensions matching the 2450 coin cells was used for the impedance measurement; the coin cell was held between the stainless steel electrodes placed into a Neslab RTE-9DD bath with an ethylene glycol water medium. A chromel–alumel thermocouple was positioned so that the tip was close to the cell environment and the temperature was monitored by a digital temperature controller. The cell was equilibrated at each temperature for at least 15 min before the measurement on a Solartron 1250 frequency response analyzer.

#### 2.3.5. Cyclic voltammetry

Cyclic voltammograms were recorded on a PAR model 173 potentiostat/galvanostat, model 176 current to voltage converter and a model RE 008 XY recorder using a home-assembled cell. The working electrode consisted of a gold foil ( $2.25 \times 10^{-4}$  m<sup>2</sup> area) onto which the sample mixed with 25 wt.% graphite was pressed. For the sake of comparison, the cyclic voltammogram of birnessite prepared by the brushing technique [16] was also registered. The birnessite prepared by the latter technique was scraped from the substrate and the procedure was repeated until sufficient amount of the material was collected.

#### 2.3.6. Magnetoresistance measurement

The magnetoresistance measurements were made on a dc magnetic susceptibility Faraday balance suitably home modified for holding the sample for magnetoresistance measurement. The balance was attached to a Keithley 224 programmable current source, a Keithley 182 sensitive digital voltmeter and a Lake Shore Cryotronics temperature controller. The end-of-discharge product was scraped from the current collector and dried at 353 K in an air oven. It was then washed under a stream of water when the lighter carbon particles were removed. It was then heat treated at 373 K for 12 h. Then the material was sealed under vacuum and heated to 1373 K for 24 h and left to cool in a horizontal position.  $\text{La}_{0.75}\text{Ca}_{0.25}\text{MnO}_3$  was used as a standard colossal material.

### 3. Results and discussion

#### 3.1. Characterization of birnessite

##### 3.1.1. XRD pattern

XRD analysis provides a convenient method of characterizing birnessites because XRD pattern of a typical birnessite material (powder diffraction standard file no. 23-1046) will be dominated by two major peaks at 7.0 Å is of great importance and represents the adjacent layer Mn–Mn distance [21]. The powder X-ray diffraction pattern of the manganese oxide prepared by the present hydroxylamine– $\text{KMnO}_4$  reaction shown in Fig. 2 (curve a) is characteristic of a layered birnessite structure with an interlayer spacing of 7.0 Å. Calcination temperature appears to exert a profound influence on the interlayer spacing. The xerogel that has been calcined at 473 K instead of 673 K shows a  $d$  spacing of 10 Å (Fig. 2, curve b). Widening of the interlayer spacing could possibly be associated with the formation of busenite, a hydrated form of birnessite [2–4,22,23]. On the other hand, heat treatment of the sample at 873 K gives an XRD pattern having a  $d$  value of 5.5 Å (Fig. 2, curve c) typical of a dehydrated birnessite [24–27]. The dehydrated sample upon equilibration with water for 74 h exhibits an XRD pattern having 10-Å interlayer spacing. This observation indicates that hydration and dehydration of birnessites is a reversible process and water molecules are held up as an interlayer sheet.

##### 3.1.2. Auger electron spectra

The Auger electron spectrum of potassium birnessite (Fig. 3) shows a signal (LMM) at 252 eV and another signal (KLL) at 503 eV. The signals, respectively, represent potassium and oxygen. The two LMM signals immediately following the oxygen signal and occurring at 542 and 589 eV are characteristic of manganese [17]. The XRD

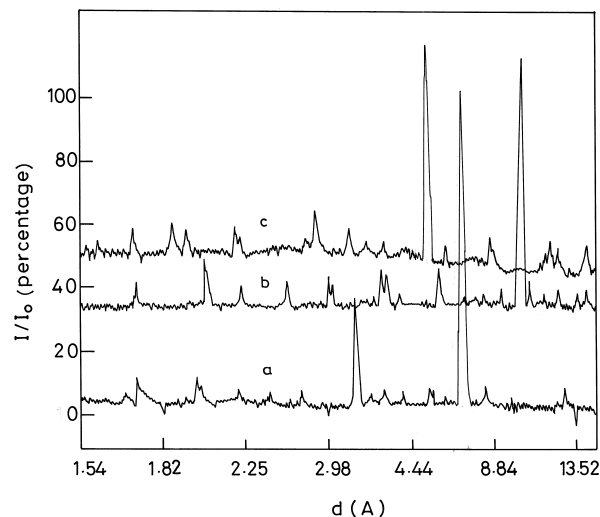


Fig. 2. Comparative XRD pattern of hydrated (curve b) and dehydrated (curve c) forms of birnessite. The scale on the Y-axis corresponds to curve a, i.e., of birnessite.

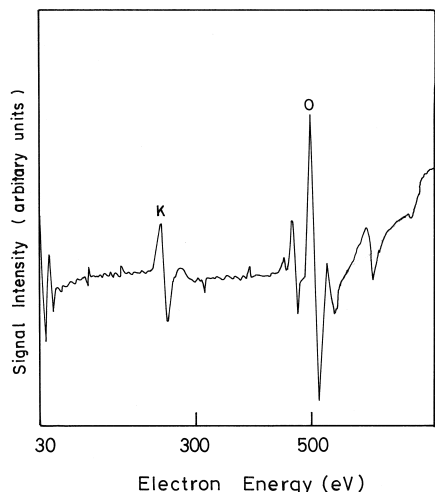


Fig. 3. Auger electron spectrum of potassium birnessite.

and the Auger electron spectral patterns together support that both potassium and water are held in the interlayer region of potassium birnessite.

### 3.1.3. Impact of reaction conditions on birnessite preparation

Synthesis of birnessite from hydroxylamine–potassium permanganate system is strongly influenced by the reaction conditions, particularly, hydroxylamine:KMnO<sub>4</sub> ratio and pH exert a profound influence. A pH of 10 and a hydroxylamine:KMnO<sub>4</sub> of 4 (or 5):1 favour the formation of a gel. At the 4 (or 5):1 ratio of hydroxylamine:KMnO<sub>4</sub>, if the alkalinity is decreased, the system changes from the formation of a gel to a flocculent mass (pH 8–9) and then to a precipitate (pH 6–8). At pH 10, if the hydroxylamine:KMnO<sub>4</sub> ratio is altered by decreasing the hydroxylamine content, a similar shift from gel to precipitate formation is noticed. The precipitate has been identified by XRD to be Mn<sub>2</sub>O<sub>3</sub> (Fig. 4). The observations are listed in Table 1.

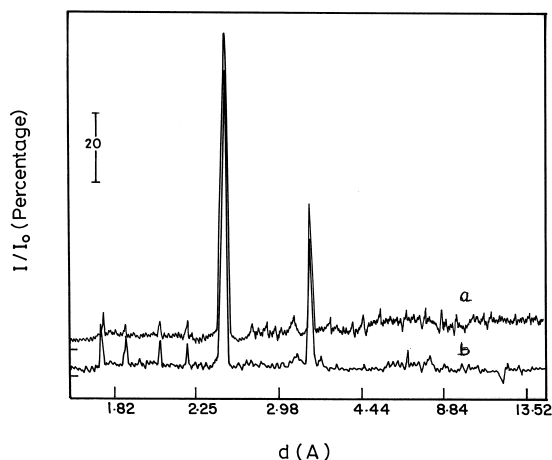


Fig. 4. (a) XRD pattern of the precipitate isolated from the reaction of 2:1 of hydroxylamine: KMnO<sub>4</sub> at pH 10 (b) XRD pattern of  $\alpha$ -Mn<sub>2</sub>O<sub>3</sub>.

Table 1

Influence of the reaction conditions on the sol–gel redox reaction of KMnO<sub>4</sub> and hydroxylamine

KMnO <sub>4</sub> : hydroxylamine ratio	pH	Initial phase	Product
5:1	10–11	gel	birnessite
4:1	10–11	gel	birnessite
5:1	8–9	flocculent gel	birnessite
5:1	6–7	precipitate	Mn <sub>2</sub> O <sub>3</sub>
5:1	3	no precipitate	
2:1	10	precipitate	Mn <sub>2</sub> O <sub>3</sub>
3:1	10	precipitate	Mn <sub>2</sub> O <sub>3</sub>
3:1	6–8	precipitate	Mn <sub>2</sub> O <sub>3</sub>

At the optimum condition of pH 10 and a hydroxylamine:KMnO<sub>4</sub> of 4 (or 5):1 ratio, the sol–gel synthesis is resistant to heating, say up to boiling. However, heating did not bring about any significant alteration in the features of the birnessite isolated.

### 3.2. Battery performance evaluation

Birnessites have a near MnO<sub>2</sub> stoichiometry. However, generally, they are known to have variable and poorly defined elemental composition [17,27]. Therefore, in the calculation of the ampere hour capacity, we have taken MnO<sub>2</sub> as the formula basis neglecting the other constituents and this assumption has been uniformly maintained for all the battery systems. In comparing the discharge performance, the discharge capacity has been expressed as percentage of the calculated ampere hour. The discharge performance of the birnessite synthesized by the above mentioned procedure in zinc-, magnesium- and lithium-based cells is shown in Fig. 5 (curves Ia, IIa, IIIa, and IVa). The birnessite as synthesized does not give good performance as a cathode in all the systems studied. But heat treatment brings about a remarkable improvement in the discharge performance of the birnessite. The discharge performance dependence on heat treatment is also presented in Fig. 5. The birnessite, which was heated at 523 K (Fig. 5, curves Ib, IIb, IIIb) in air, gave a superior performance over the untreated birnessite and a sample of birnessite that was heat treated at 673 K (Fig. 5, curves Ic, IIIc, IVb) gave a still better performance. A similar improvement in performance of the birnessite was effected by boiling the birnessite in 5% nitric acid solution (curves IIc and IVc).

The poor performance of the potassium birnessite could be explained on the basis of its structure. Desai et al. [29] who tested the suitability of the following equation to define the discharge behaviour of MnO<sub>2</sub> of different crystalline phases.

$$E = E^{\circ} + \frac{2RT}{F} \ln \frac{(1 - (1 + \alpha)r)^{(1 + \alpha)}}{r(1 + \alpha)r}$$

where  $0 < r < 1$  and  $\delta \rightarrow 0$ ;  $r$  is considered to be an independent variable;  $\alpha$  is the term introduced to account

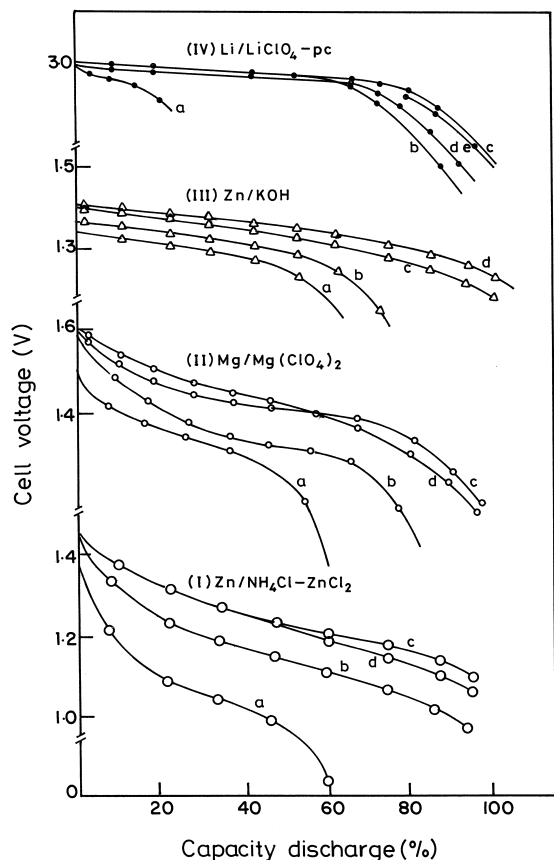


Fig. 5. Battery performance tests. Ia, IIa, IIIa and IVa birnessite as synthesized. Ib, IIb and IIIb birnessite heat treated at 523 K. Ic, IIIc and IVb, heat treatment at 673 K. IVc and IIc acid treatment by boiling in 5%  $\text{HNO}_3$  for 5 days. Id, IId, IIId and IVe Bi-birnessite. IVd birnessite by Kanoh procedure.

for the number of sites not available for proton insertion. The value of  $\alpha$  is obtained from the relation.

$$\gamma_{\max} = \frac{1}{1 - \alpha}$$

where  $\gamma_{\max}$  is the value at the end of the homogeneous reduction and is obtained from observed discharge curve.

It was found that the most marked deviation from the theoretical value was shown by  $\delta\text{-MnO}_2$ . Furthermore, they showed that  $\delta\text{-MnO}_2$  fails to fit into a few other theoretical models as well. According to Giovanoli [30],  $\delta\text{-MnO}_2$  is not a true  $\text{MnO}_2$  modification but a cognate member of the  $\text{MnO}_2$  family. It was shown by Feng et al. [31] that birnessite-type manganese oxides could be transformed into tunnel structures.

The work of Yao et al. [11], however, showed Bi- and Pb- birnessites to be superior battery positives, with respect to reversibility, capacity retention and cycle life as compared with conventional manganese dioxides. These varieties have no inherent limitation to their cycle life even under conditions of deep discharge reaching 80%–95% of their theoretical two electron capacity in each cycle. The unique properties of these materials include also the capacity of high current drains and insensitivity to over dis-

charge and overcharge. In the light of these findings of Yao et al., the Bi- and Pb- exchanged sodium birnessites prepared by the present hydroxylamine route were subjected to battery discharge tests. The discharge curves in the different systems studied are shown by curves Id, IId, IIIId and IVe in Fig. 5. It is evident that the performance is superior when compared with the potassium counterpart. Furthermore, when the Bi- and Pb-exchanged birnessites were investigated in laboratory cells constructed and tested by following Yao et al.'s procedure [11], they yielded, respectively, 240 and 260 cycles. Whereas only 70 cycles have been obtained for the potassium birnessite under the same conditions. Attempts have also been made to effect lithium insertion into the birnessite both by aqueous [32] and nonaqueous [33] methods and the resulting material exhibited very high reversible capacity at high current densities of the order,  $0.5 \text{ mA/cm}^2$ . Lithium insertion into the birnessite has been proven by atomic absorption and the material thus marks the beginning of a series of readily synthesizable lithium manganese dioxide which have potential application in rechargeable lithium batteries. Manthiram and Kim [34] discussed that the presence of intimately mixed second phase of  $\text{Na}_x\text{MnO}_2$  in lithium manganese dioxides is extremely beneficial to the capacity retention of lithium cells.

Yao et al. [11] have discussed in detail the beneficial effects of introducing  $\text{Bi}^{3+}$  and  $\text{Pb}^{2+}$  into the birnessite. Among other factors, they have stressed the significance of structural factors and conductivity of the intermediates formed during discharge. The results obtained in the present study are in agreement with Yao et al.'s findings and support that Bi- and Pb-exchanged birnessites are excellent materials for both the primary and secondary battery systems.

### 3.3. Influence of temperature on EPR pattern

Heat treatment as a route to convert one crystalline form of manganese dioxide to another is a well-established technique and it is worth mentioning here about two modifications of  $\text{MnO}_2$ , viz., the alpha and the beta forms. The alpha form hollandite-type  $\text{MnO}_2$  [35] and beta forms [37] are found to be suitable for non-aqueous lithium rechargeable batteries [36a,36b].

Alpha  $\text{MnO}_2$  is actually a non-stoichiometric oxide of formula,  $\text{MnO}_{2-\alpha}$ . The  $\alpha$  part is composed of  $\text{H}^+$  ions in constituent water which interact with manganese oxide lattice and contains  $\text{K}^+$  ions in its  $2 \times 2$  tunnels [37]. The conversion of birnessite into the alpha form thus seems to be a readily anticipated one during the heat treatment at 523 K and that the conversion has taken place is supported by the EPR spectrum of the heat treated sample shown in Fig. 6 (curve a). An admixture of the absorption spectra due to  $M_s = -1/2$  and  $M_s = +1/2$  exhibited in the EPR pattern (Fig. 6, curve a) is indicative of spin orbit coupling expected of  $\alpha\text{-MnO}_2$ . Curve b in Fig. 6 represents the EPR pattern of birnessite that was heat treated at 673 K (24 h).

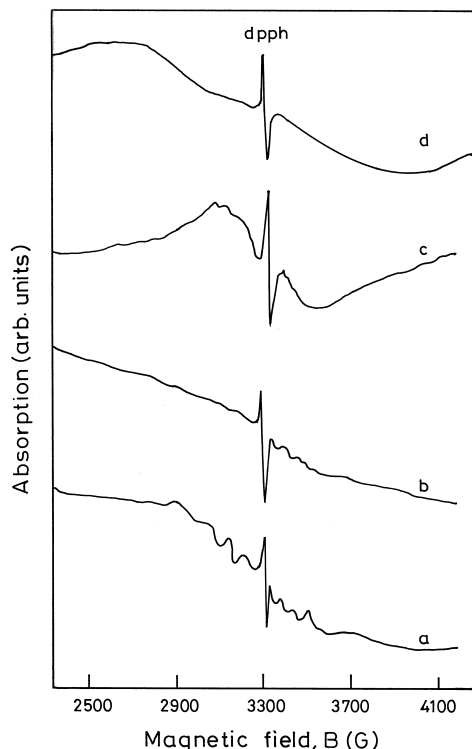


Fig. 6. EPR spectra of birnessite heat treated (a) 383 K (b) 523 K (c) 623 K (d) untreated.

The pattern expresses an admixture of  $M_s = -5/2$  and  $M_s = -3/2$  levels [38]; the broadened nature [39] of the curve is characteristic of beta  $\text{MnO}_2$ . Evidence from several lines of works [40] suggests that beta  $\text{MnO}_2$  is the most stable form of manganese dioxide and that other types can be converted to it by suitable treatment. A sample of birnessite that was heat treated in air at 383 K

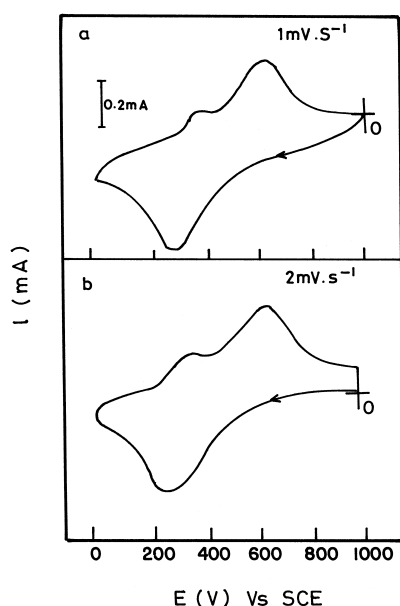


Fig. 7. Cyclic voltammogram of birnessite of (a) present method (b) Kanoh method. Medium: 0.1 M KCl; pH 7.2.

for 5 days gave an EPR pattern similar to that of a gamma- $\text{MnO}_2$  (Fig. 6 curve c).

### 3.4. Cyclic voltammetry

The cyclic voltammogram of untreated birnessite in 0.1 M KCl in a buffered (Britton Robinson buffer) solution of pH 7.2 is shown in Fig. 7a. The pattern is identical with the cyclic voltammogram of birnessite prepared by the brushing technique of Kanoh et al. [20] shown in Fig. 7b. The cyclic voltammograms of the birnessite (that has been boiled in dilute  $\text{HNO}_3$  (5%) for 5 days) in 1 M  $\text{LiClO}_4$ /di-oxalane electrolyte at 393 K is shown in Fig. 8. A prominent redox couple is seen in the cyclic voltammogram with an anodic peak potential  $E_{pa}$  at 3.35 V and a cathodic peak potential  $E_{pc}$  at 2.75 V. The couple corresponds to the reduction of  $\text{Mn}^{4+}$  ions to  $\text{Mn}^{3+}$  [41]. The couple exhibits a constancy of the  $E_p$  values at different sweep rates with  $i_{pa} = i_{pc}$  and  $\Delta E_p = 55$  mV characteristic of 1e process. In birnessites, the oxidation state of manganese normally falls between 3.6 and 3.8 [1,3,28] which represents a predominance of Mn(IV) with minor amounts of Mn(III). There has also been some speculation over the presence of Mn(II) [1,3]. The shoulders exhibited by the cyclic voltam-

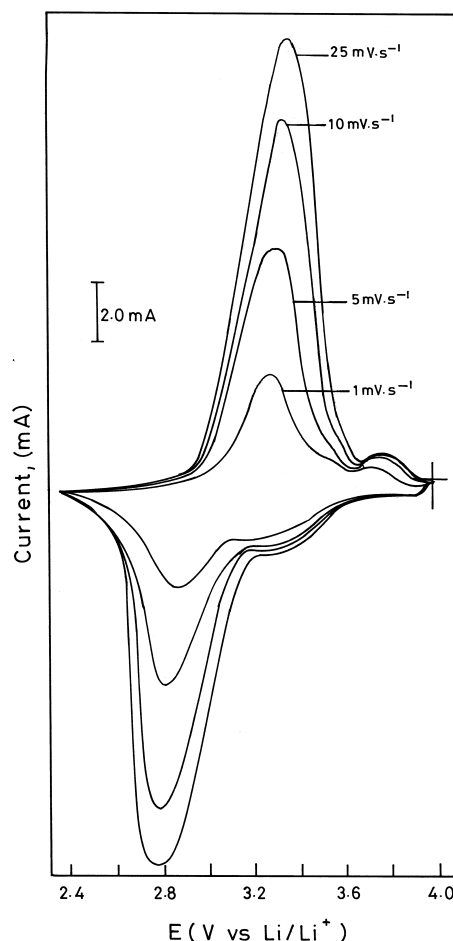


Fig. 8. Cyclic voltammogram of birnessite that has been treated by boiling in 5%  $\text{HNO}_3$  for 5 days; in 1 M  $\text{Li/Li}^+$  couple at 393 K.

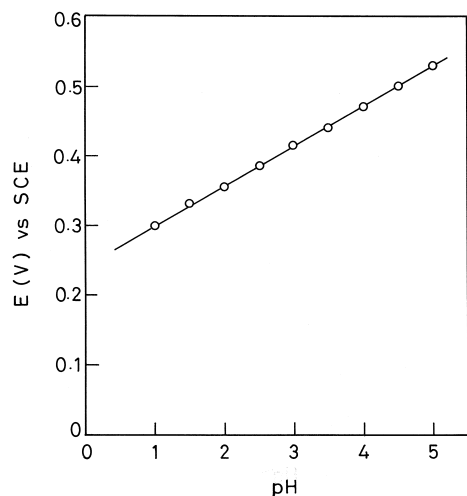


Fig. 9. Potential-pH diagram for birnessite in Britton-Robinson buffer.

mogram in Fig. 8 might be representative of such coexistent species which, however, require a detailed study. pH dependence of the potential of the potassium birnessite electrode was measured in buffered solutions (Britton-Robinson buffer); a Nernstian response was observed (Fig. 9) with a slope of 58.96 mV, showing that  $H^+$  is electrochemically active towards birnessites [20].

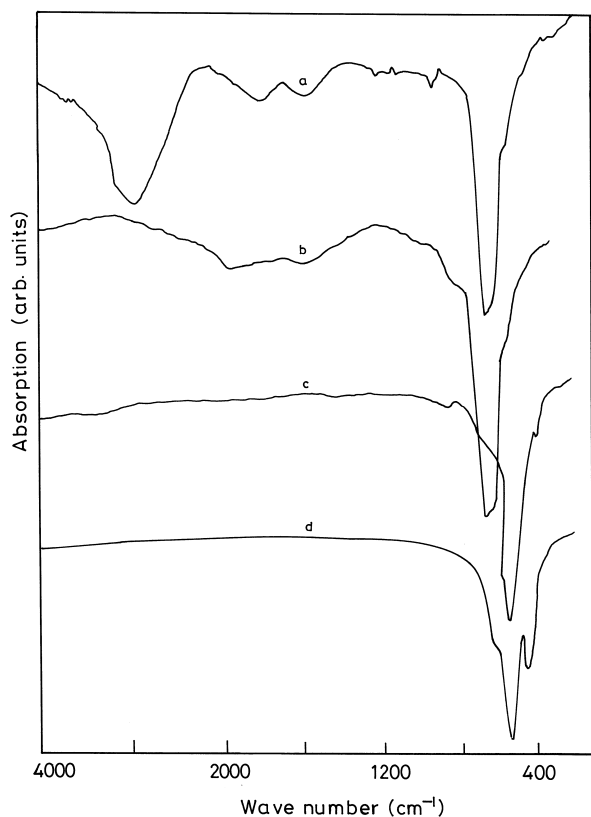


Fig. 10. IR spectra of birnessite heat treated at different temperatures (a) untreated, (b) 383 K in air for 3 days, (c) 473 K in air for 10 h, (d) 673 K in air for 10 h.

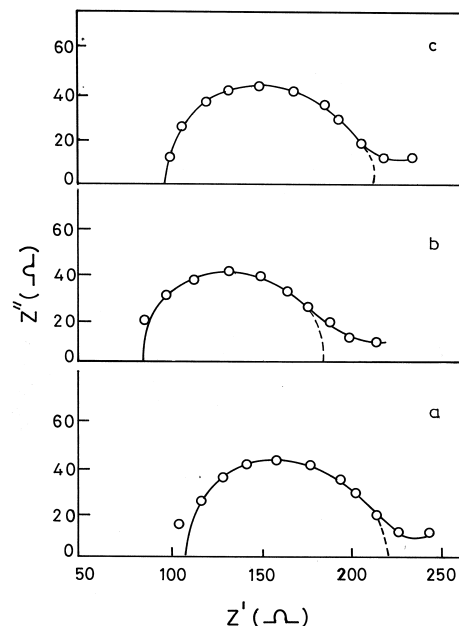


Fig. 11. Impedance pattern Li cell at (a) 295 K (b) 303 K Cl pattern for Kanoh birnessite.

### 3.5. Influence of heat treatment on IR pattern

The improvement in the electrochemical activity of manganese oxide by heat treatment [42] can be correlated to the change in its water content. In general, three kinds of water have been observed in manganese dioxides [43]. They are: (i) absorbed water, (ii) interlayer water, and (iii) constituent water of the lattice. These waters are, respectively, discharged in the temperature range of 297–378, 423–523 and 378–773 K. The constituent water is essential for the stability of the lattice [44] and when it is released, collapse of the lattice begins to take place eventually resulting in initiation of amorphisation of the material [37].

When potassium birnessite was heated to 773 K through different intermediary steps, there were distinct changes in the IR spectral pattern corresponding to different degrees of release of water (Fig. 10). The changes occurring in the 400–750  $cm^{-1}$  should correspond to changes in manganese oxide lattice. Reported evidence shows that when heated to 393 K in air, the delta form is converted into the gamma form [45], whereas upon heat treatment at 423–673 K, it is converted into the beta form, similarly, heating the delta form in dilute acid solution also effects the conversion to the alpha or the gamma form [46,47]. In general, chemical manganese dioxides exhibit the lengthening of

Table 2  
Temperature dependence of impedance parameters of the lithium cell

Temp. (K)	$R_{sol}$ ( $\Omega$ )	$R_{act}$ ( $\Omega$ )	$C_{dl}$ ( $\mu F cm^{-2}$ )	$i_0$ ( $mA cm^{-2}$ )
308	90	116	2.7	0.089
295	115	118	2.3	0.076

the Mn–O bond [48,49] and probably heat treatment alters certain features of the Mn–O bonding and dispersion of phase transition. However, further analysis is essential to arrive at any definite information on the IR spectral changes in the 400–750  $\text{cm}^{-1}$  region.

### 3.6. Impedance measurements

Fig. 11 shows the complex plane plots of the Li–birnessite cell. The birnessite was not used as synthesized in the cathode, but it was heat treated at 623 K prior to cathode fabrication. The anode performance is represented by the high frequency part of the complex plane plots. We observed  $C_{dl}$  values in the range 2.7–5.9  $\mu\text{F cm}^{-2}$  (Table 2) and the  $i_0$  values are in the range 0.089–0.025  $\text{mA cm}^{-2}$ . Further,  $i_0$  increases with temperature with concomitant decrease in the solution resistance and  $R_{act}$ . The beneficial effect of higher temperature on the performance of lithium batteries is well known. This is because the viscosity of the electrolyte decreases and diffusion is favored. In general, the impedance pattern of the Li–birnessite cell is similar to that of Li– $\text{MnO}_2$  cells studied by other workers [50–52]. It is reasonable to state that because of the prior heat treatment, conversion of the  $\delta\text{-MnO}_2$  of the birnessite into an electrochemically more active form might have occurred. However, dehydrated birnessite prepared by following the brushing procedure of Kanoh et al. [20] also showed a similar impedance pattern (Fig. 11, curve c) at room temperature.

### 3.7. Magnetoresistance measurements

As manganite perovskites are known for giant magnetoresistance [53], we became interested in examining the magnetoresistance pattern of potassium birnessite in its discharged forms. In a preliminary study, we found that about 50% discharged product of the magnesium/potassium birnessite/ $\text{Mg}(\text{ClO}_4)_2$  cell showed a magnetoresistance pattern similar to that of a colossal magnetoresistance material for instance,  $\text{La}_{0.75}\text{Ca}_{0.25}\text{MnO}_3$  (Fig. 12). Mixed valence Mn(III)–Mn(IV) perovskites are materials

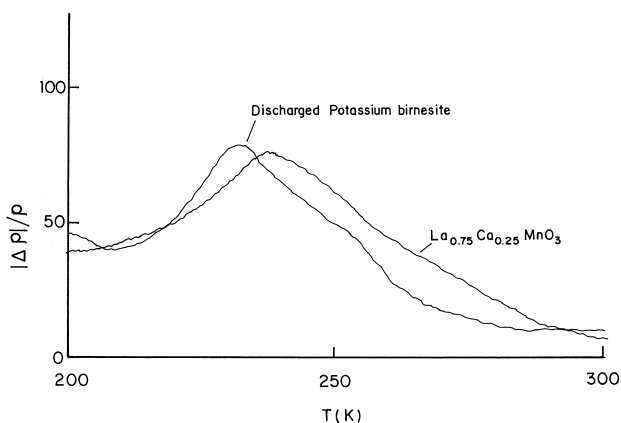


Fig. 12. Magnetoresistance pattern of the 50% discharged product of  $\text{Mg}/\text{Mg}(\text{ClO}_4)_2$ /heat treated (523 K) birnessite cell.

presently being actively investigated [54] because they have been found to change dramatically their electric resistance in the presence of an applied magnetic field. Birnessites are known to have mixed valent [Mn(III)–Mn(IV)] manganese; incorporation of ions such as  $\text{Mg}^{2+}$ , and some  $\text{Ba}^{2+}$  and chromate-derived ions (from the corrosion inhibitor) into the discharged product is also a possibility. A detailed study is essential for an understanding of the mechanism of operation of giant magnetoresistance in the discharged manganese oxides. At present, it can only be said that magnetoresistance measurement can be examined for its utility in identifying the battery discharge status of manganese oxides.

## 4. Conclusion

Hydroxylamine, a well-known reducing agent brings about an efficient reduction of potassium permanganate to birnessite, a layered manganese dioxide. During the reaction, first, a sol is formed which turns into a gel that ultimately yields birnessite after drying and calcination. Conventional sol–gel techniques that make use of alkoxide precursors produce gels from the hydrolyzed metal alkoxides. The hydroxylamine– $\text{KMnO}_4$  system involves only the reduction of the permanganate ion. It is reasonable to presume that the gel formation is assisted by hydroxylamine and OH ions of the alkaline medium. The relatively high concentration of hydroxylamine required for gelation indicates availability of partially oxidized or unoxidized hydroxylamine in the medium. A network of manganese oxide and hydroxylamine moieties might result in gelation. A similar mechanism of formation of ‘‘manganese dioxide jellies’’ have been reported during the reaction between  $\text{KMnO}_4$  and sugars [16,17,55–57] and also between  $\text{KMnO}_4$  and fumaric acid [15]. A noteworthy difference between the birnessite derived from glucose– $\text{KMnO}_4$  sol–gel system and the hydroxylamine  $\text{KMnO}_4$  sol–gel system is that in the former route [17], the birnessite shows some resistance to hydration after it has been dehydrated, whereas the latter route is seen to yield birnessites that undergo hydration and dehydration without much difficulty. This observation reemphasizes the established feature associated with manganese oxides, that is, the structure of a particular product does depend largely on the type of process by which it was prepared; for example, Desai et al. [29] observed that even a slight change in the method of preparation of chemical manganese dioxide (CMD) by  $\text{NaClO}_3$  route does alter its homogeneous phase reduction range. Jiang et al. [58] showed that the activity of activated  $\text{MnO}_2$  is affected greatly by the concentration of  $\text{H}_2\text{SO}_4$  used for activation.

The birnessite as synthesized by the present  $\text{KMnO}_4$ –hydroxylamine showed poor battery discharge activity. On the contrary, ion exchange with  $\text{Bi}^{3+}$  or  $\text{Pb}^{2+}$ , heat treatment or boiling in dilute acid, improved the battery performance in all the systems, viz., zinc-, magnesium- and

lithium-based cells. This improvement is owing to the conversion of the sodium/potassium birnessite into electrochemically more active forms of manganese oxide. Using the sodium precursor, it was possible to prepare the  $\text{Bi}^{3+}$ -,  $\text{Pb}^{2+}$ - and  $\text{Li}^+$  exchanged birnessites and these varieties showed excellent capacity retention and cyclability. Facile lithium insertion into manganese dioxides is advantageous in view of the importance of the application in lithium rechargeable cells. The preliminary investigation made in the present work on the magnetoresistance of discharged manganese oxide necessitates further work in this direction. Similarly, the changes in the IR spectral pattern of manganese oxide (particularly in the 400–750  $\text{cm}^{-1}$  region) produced by heat treatment deserve further examination. It is worthwhile to examine the suitability of these techniques for the evaluation of the electrochemical activity of manganese oxides.

### Acknowledgements

The authors are thankful to Shri. C. Sankaran, Scientist-in-Charge, National Metallurgical Laboratory, Madras Centre, for the help in furnace facility, to Prof. Rama Rao, Physics Dept. IIT Madras, Chennai, and to Prof. S. Subramanian, RSIC, IIT Madras, Chennai, for the help in recording the XRD pattern and Auger spectral measurements, to Dr. A. Veluchamy and M.R. Balasubramanian, CECRI, for the guidance in the study of lithium cells and to Prof. B. Viswanathan, Dept. of Chemistry, IIT Madras, Chennai, for the help and encouragement in undertaking the magnetoresistance measurement.

### References

- [1] D.C. Golden, J.B. Dixon, C.C. Chen, *Claus Clay Miner.* 34 (1986) 511.
- [2] P. Strobel, J.C. Charenton, M. Lenglet, *Rev. Chim. Miner.* 24 (1987) 199.
- [3] Q. Peng, H. Kanoh, Y. Maiyai, K. Ooi, *Chem. Mater.* 7 (1996) 1722.
- [4] R.M. McKenzie, *Miner. Mag.* 38 (1971) 493.
- [5] R.G. Burns, V.M. Burns, in: G.P. Glasby (Ed.), *Marine Manganese Deposits*, Chap. 7, Elsevier, New York, 1977.
- [6] S. Bach, J.P. Pereira-Ramos, N. Baffier, R. Messina, *Electrochim. Acta* 38 (1993) 1695.
- [7] S. Bach, J.O. Pereira-Ramos, N. Baffier, *Electrochim. Acta* 38 (1993) 1675.
- [8] P. Strobel, C. Mouget, *Mater. Res. Bull.* 28 (1993) 93.
- [9] F. Lecras, S. Rohs, M. Anne, P. Strobel, *J. Power Sources* 54 (1995) 1675.
- [10] A.R. Armstrong, P.G. Bruce, *Nature* 381 (1996) 499.
- [11] Y.F. Yao, N. Gupta, H.S. Wroblowa, *J. Electroanal. Chem.* 223 (1987) 107.
- [12] H.S. Wroblowa, in: O.J. Murphy, S. Srinivasan, B.E. Conway (Eds.), *Electrochemistry in Transition*, Plenum, New York, 1992, p. 147.
- [13] M.A. Dzicciuch, N. Gupta, H.S. Wroblowa, J.T. Kummer, U.S. Patent No. 4,451,543, May 29, 1984.
- [14] R.M. Jones, *Fundamental Principles of Sol–Gel Technology*, London, IOM, 1989.
- [15] S. Bach, J.P. Pereira-Ramos, N. Baffier, *Solid State Ionics* 80 (1995) 151.
- [16] S. Ching, J.A. Landrigan, M.L. Jorgensen, N. Duna, S.L. Suib, C.L.O. Young, *Chem. Mater.* 7 (1995) 1604.
- [17] S. Ching, D.J. Petrovay, M.L. Jorgensen, *Inorg. Chem.* 36 (1997) 883.
- [18] S.A. Barket, E.J. Bourne, R.M. Pinkard, D.H. Whiften, *J. Chem. Soc.*, (1995) 802.
- [19] N.C. Cahoon, in: N.C. Cahoon, G.W. Heise (Eds.), *The Primary Battery*, Vol. II, Chap. 1, Wiley, New York, 1976.
- [20] H. Kanoh, W. Tang, Y. Makita, K. Ooi, *Langmuir* 13 (1997) 6845.
- [21] R.M. Potter, G.R. Rossman, *Am. Miner.* 64 (1979) 199.
- [22] R.G. Burns, V.M. Burns, *Phil. Trans. R. Soc. London A* 286 (1977) 283.
- [23] J.E. Post, D.R. Veblen, *Am. Miner.* 75 (1990) 477.
- [24] R. Chen, P. Zavaliji, M.S. Whittingham, *Chem. Mater.* 8 (1996) 1275.
- [25] P. Le Goff, N. Baffier, S. Bach, J.P. Pereira-Ramos, P. Messina, *Solid State Ionics* 61 (1993) 309.
- [26] S. Hirano, R. Narita, S. Naka, *Mater. Res. Bull.* 19 (1984) 1229.
- [27] S. Bach, J.P. Pereira-Ramos, N. Baffier, *J. Solid State Chem.* 120 (1995) 70.
- [28] P. Strobel, J.C. Charenton, M. Lenglet, *Rev. Chim. Miner.* 24 (1987) 199.
- [29] B.D. Desai, R.A.S. Dhume, V.N.K. Dalal, *J. Appl. Electrochem.* 18 (1988) 62.
- [30] R. Giovanoli, *Chimia* 23 (1969) 472.
- [31] Q. Feng, K. Yamasaki, K. Yanagisawa, K. Ooi, *J. Mater. Sci. Lett.* 15 (1996) 963.
- [32] J. Kim, A. Manthiram, *Nature* 390 (1997) 265.
- [33] J. Kim, A. Manthiram, *Electrochem. Solid State Lett.* 1 (1997) 207.
- [34] A. Manthiram, J. Kim, *Trans. SAEST* 34 (1999) 1.
- [35] Q. Feng, H. Kanoh, K. Ooi, M. Tani, Y. Nakacho, *J. Electrochem. Soc.* 141 (1994) 135.
- [36a] U.N. Khodarev, *Electrochimica* 27 (1991) 1046.
- [36b] P.G. Bruce, *Chem. Commun.*, (1997) 1817.
- [37] I. Ohzuku, M. Kitagawa, K. Sawami, L. Hirai, *J. Electrochem. Soc.* 138 (1991) 360.
- [38] M.V. Ananth, K. Dakshinamurthi, *J. Mater. Chem.* 7 (1997) 51.
- [39] H. Huang, P.G. Bruce, *J. Electrochem. Soc.* 141 (1994) 76.
- [40] N.C. Cahoon, in: N.C. Cahoon, G.W. Heise (Eds.), *The Primary Battery*, Vol. II, Wiley, New York, 1976, p. 92.
- [41] N.S. Bach, N. Baffier, *J. Power Sources* 43 (1993) 569.
- [42] H. Tamura, in: S. Yoshikawa (Ed.), *Electrochemistry of Manganese Dioxide and Manganese Dioxide Batteries in Japan*, U.S. Branch Office, Electrochem. Soc. Japan, Cleveland, OH, 1973, p. 189.
- [43] R. Giovanoli, *Thermochem. Acta* 234 (1994) 303.
- [44] G. Buttler, H.R. Thirsk, *Acta Crystallogr.* 5 (1992) 288.
- [45] G. Gattow, O. Glemser, *Z. Anorg. Allg. Chem.* 121 (1961) 369.
- [46] K.H. Maxwell, H.R. Thirsk, *J. Chem. Soc.*, (1995) 4057.
- [47] W. Peitknecht, E. Golvato, *J. Res. Natl. Bur. Stand.* 41 (1948) 589.
- [48] J. Amiel, J. Brenet, G. Rodier, Report at Conf. on the Plariazation of Matter, Paris, 4–9 April, 1949.
- [49] J. Amiel, J. Brenet, R. Rodies, *C. R. Acad. Sci.* 227 (1948) 1356.
- [50] R. Janakiraman, K. Gopalakrishnan, P.N.N. Namboodiri, R. Gangadharan, *Bull. Electrochem.* 7 (1991) 529.
- [51] J.R. Sandifer, M.R. Suchanski, *J. Appl. Electrochem.* 14 (1984) 329.
- [52] R.F. Scarr, *J. Electrochem. Soc.* 117 (1970) 295.
- [53] C.W. Searle, S.I. Wang, *Can. J. Phys.* 47 (1969) 2703.
- [54] C.N. Rao, *Chem. Eur. J.* 2 (1996) 499.
- [55] E.J. Witzmann, *J. Am. Chem. Soc.* 35 (1915) 1079.
- [56] E.J. Witzmann, *J. Am. Chem. Soc.* 37 (1917) 25.
- [57] S. Prakash, N.R. Dhar, *J. Indian Chem. Soc.* 7 (1930) 41.
- [58] W.S. Li, L.C. Jiang, G.Y. Xie, X. Jiang, *J. Power Sources* 58 (1996) 235.